

Eccentricity Growth Rates of Tidally Distorted Discs

Stephen H. Lubow^{1,2}

¹*STScI, 3700 San Martin Drive, Baltimore, MD 21218, USA*

²*Institute of Astronomy, Madingley Road, Cambridge, CB3 0HA, UK*

14 February 2022

ABSTRACT

We consider discs that orbit a central object and are tidally perturbed by a circular orbit companion. Such discs are sometimes subject to an eccentric instability due to the effects of certain resonances. Eccentric instabilities may be present in planetary rings perturbed by satellites, protostellar discs perturbed by planets, and discs in binary star systems. Although the basic mechanism for eccentric instability is well understood, the detailed response of a gaseous disc to such an instability is not understood. We apply a linear eccentricity evolution equation developed by Goodchild and Ogilvie. We explore how the eccentricity is distributed in such a disc and how the distribution in turn affects the instability growth rate for a range of disc properties. We identify a disc mode, termed the superhump mode, that is likely at work in the superhump binary star case. The mode results from the excitation of the fundamental free precession mode. We determine an analytic expression for the fundamental free mode precession rate that is applicable to a sufficiently cool disc. Depending on the disc sound speed and disc edge location, other eccentric modes can grow faster than the superhump mode and dominate.

Key words: accretion, accretion discs — instabilities — (stars:) binaries (including multiple): close — planet disc interactions — planets: rings — methods: numerical

1 INTRODUCTION

Consider a gaseous disc that orbits about a central object. If the disc is tidally perturbed by a circular orbit companion, but the disc is otherwise circular, then its response at certain (Lindblad) resonance locations can be quite strong and result in the launching of waves that extract energy and angular momentum from the companion (Goldreich & Tremaine 1979). If the perturber were to be removed, the disc would settle back to a circular state, with its mass having been rearranged from its initial state by the resonant torques. For discs that are slightly eccentric, additional resonances arise. Some of these resonances have the property that they can cause the disc eccentricity to grow exponentially in time, even though the perturber is on a circular orbit. In this case, if the perturber were to be removed, the disc would be in an eccentric state. The process by which eccentricity growth occurs in a fluid disc can be understood through a mode-coupling mechanism (Lubow 1991a; hereafter L91). The instability can also be understood in terms of particle dynamics with dissipation (Borderies, Goldreich, & Tremaine 1983, Ogilvie 2007). Such instabilities may explain the eccentricities of planetary rings perturbed by satellites (Borderies et al 1983), the eccentricities of circumstellar discs

perturbed by planets or brown dwarfs (Papaloizou, Nelson, & Masset 2001, Kley & Dirksen 2005, D’Angelo, Lubow, & Bate 2006), and eccentricities in discs of cataclysmic binaries (Whitehurst 1988, Lubow 1991b, Osaki 1996), and X-ray binaries (Haswell et al. 2001, Neil, Balyn, & Cobb 2007).

In this paper, we will mainly consider the superhump binary case which has been studied, both observationally and theoretically. We will generalise the results somewhat to cover cases involving warmer (larger dimensionless disc thickness) protostellar discs. The initial observational evidence for eccentric discs came from an analysis of a drifting feature, the superhump, in the light curves of extreme mass ratio cataclysmic binaries that undergo unusually strong outbursts called superoutbursts (Warner 1975). The period of the superhump feature is slightly longer than the binary orbit period. The drifting feature in the light curve was attributed to an eccentric prograde precessing disc (Vogt 1982, Osaki 1985). The prograde precession is due to the gravitational effects of the companion that causes departures of disc streamlines from closed Keplerian ellipses. Weaker retrograde effects occur due to gas pressure (Lubow 1992, Murray 2000). Simulations by Whitehurst (1988) revealed an eccentric instability that can be understood through the effects of the 3:1 eccentric Lindblad resonance (L91). Many

arXiv:1004.4156v1 [astro-ph.SR] 23 Apr 2010

observational studies have supported the idea that the disc is eccentric (e.g., Osaki 2003, Patterson 2005).

Several particle based simulations (SPH or something similar) of discs in binaries revealed properties of the instability and the disc precession (see, e.g., Smith et al 2007). For many years, simulations carried out by grid-based codes were unable to find this instability and cast some doubt on the eccentric disc model (e.g., Heemskerk 1994, Stehle 1999). However, Kley, Papaloizou, & Ogilvie (2008) recently reported finding this instability with a grid-based code and showed that its properties largely agree with theoretical expectations of the mode-coupling model. However, some properties of the instability revealed by these simulations were not predicted by the L91 model, such as the dependence of the growth rate on the disc sound speed.

The L91 model determined the eccentricity growth rate for a ring of gas having uniform eccentricity. It was generalised to a full disc, again assuming the eccentricity is uniformly distributed. However, it is by no means obvious that the disc eccentricity would always be uniform. The distribution of eccentricity has an important influence on the eccentricity growth rate. The resonance provides a certain rate of angular momentum and energy input, resulting in an eccentricity growth. But if this angular momentum and energy input is shared over a broad eccentric region of the disc, then we expect the eccentricity growth rate to be smaller than if the region is narrow. In fact, the L91 model predicts that the growth rate to vary as roughly the inverse of the radial width of the eccentric region.

Important progress in understanding the disc eccentricity distribution and its effects on the growth rate was made by Goodchild & Ogilvie (2006; hereafter GO06). They derived differential equations for the radial distribution and growth rate of eccentricity, subject to the eccentric instability caused by the resonance. Their results for superhump binaries, involving the 3:1 resonance, indicated that the disc eccentricity growth rate was lower than expected from simulations and observations. The reason for the small growth rate is that the mode they analysed has a low amplitude near the resonance. Consequently, the resonance was ineffective in providing eccentricity growth. We therefore have a puzzle that a more complete modeling of the disc eccentricity evolution resulted in growth rates that are lower than expected. In this paper we re-examine the nature of the eccentricity evolution of a disc, using the GO06 equations, in an attempt to resolve this issue. In the process, we determine a more strongly excited mode that we call the superhump mode. We analyse its properties under various conditions. We also determine other modes than can dominate, under somewhat different disc conditions than are typically expected in superhump binaries.

The outline of the paper is as follows. In Section 2, we describe the eccentricity evolution equations. Section 3 specifies the standard model parameters used in the calculations. Section 4 discusses the methods to solve the eccentricity evolution equations. The results of the calculations for a variety of system parameters are described in Section 5. Section 6 contains the summary.

2 ECCENTRICITY EVOLUTION EQUATIONS

Consider a two-dimensional disc that orbits about a primary object which is located at the origin of a cylindrical coordinate system (r, ϕ) . The low-mass secondary is in a circular orbit of semi-major axis d about the central object. We apply the linearised eccentricity equations of GO06, expressed in the following form

$$i\partial_r(a(r)\partial_r E(r, t)) + ib(r)E(r, t) + J(r)s(r)E(r, t) = J(r)\partial_t E(r, t), \quad (1)$$

where $E(r, t) = e(r, t) \exp(i\varpi(r, t))$ is the complex eccentricity, for real eccentricity e and periape angle ϖ . This two dimensional approximation is valid under the assumption of vertical (perpendicular to the disc plane) hydrostatic equilibrium for a thin disc. The reduction to two dimension results from a vertically integration of three dimensional equations. We ignore the effects of viscosity on the eccentricity. For the case of no perturbing body, the nonlinear evolution of an eccentric, three dimensional, viscous disc was analysed by Ogilvie (2001).

E is related to the linear perturbations from the axisymmetric circular velocity. For the velocity expressed cylindrical coordinates as $(u'(r, t) \exp(-i\phi), v'(r, t) \exp(-i\phi))$ we have that

$$u'(r, t) = ir\Omega(r)E(r, t) \quad (2)$$

and

$$v'(r, t) = \frac{1}{2}r\Omega(r)E(r, t), \quad (3)$$

where $\Omega(r)$ is the Keplerian orbital frequency about the primary of mass M_p given by

$$\Omega(r) = \sqrt{\frac{GM_p}{r^3}}. \quad (4)$$

Quantity $J(r)$ is the disc angular momentum per unit radius divided by π and is given by

$$J(r) = 2r^3\Omega(r)\Sigma(r). \quad (5)$$

Functions $a(r)$ and $b(r)$ are given by

$$a(r) = \gamma P(r)r^3, \quad (6)$$

$$b(r) = \frac{dP}{dr}r^2 + J(r)\dot{\varpi}_g, \quad (7)$$

where $P(r)$ is the two-dimensional (vertically integrated) disc pressure, $\Sigma(r)$ is the disc surface density, and $\dot{\varpi}_g$ is the gravitational precession rate of a free particle on an eccentric orbit which is given by

$$\dot{\varpi}_g(r) = \frac{1}{4}q \left(\frac{r}{d}\right)^2 \Omega(r) b_{3/2}^{(1)} \left(\frac{r}{d}\right). \quad (8)$$

The terms involving quantities a and b describe the eccentricity propagation and precession, respectively. Quantity γ is the gas adiabatic index. Mass ratio q is the mass of the secondary (perturbing) object divided by the mass of the primary (central) object, and $b_{3/2}^{(1)}$ is the Laplace coefficient for the $m = 1$ tidal potential component associated with the perturbing object. Real function $s(r)$ is the eccentricity growth rate contribution from the eccentric instability. It is largest in a region containing the resonance that drives the instability. In the case of superhump binaries, this is the 3:1 resonance.

The surface density $\Sigma(r)$ is taken to vary smoothly from inner radius r_i to outer radius r_o and to be zero outside this range. Functions $a(r)$ and $b(r)$ vary smoothly in radius, while function $s(r)$ is localised near the resonance. For the eccentricity injection rate caused by a resonance, we generally adopt a gaussian form

$$s(r) = \frac{\chi \exp[-(r - r_{\text{res}})^2/w_{\text{res}}^2]}{\sqrt{2\pi}w_{\text{res}}}, \quad (9)$$

where r_{res} is the radius of the resonance that excites eccentricity, w_{res} is the resonance width, and χ is a measure of the resonance strength.

We consider the boundary conditions at the disc inner and outer edges located at radii r_i and r_o , respectively. Following GO06, we adopt the outer boundary condition

$$\partial_r E(r_o, t) = 0. \quad (10)$$

For a Keplerian disc, the divergence of the velocity is proportional to $\partial_r E$. Consequently, this boundary condition is equivalent to requiring that the Lagrangian density perturbation near the disc outer edge vanishes.

The inner boundary condition is taken to be

$$E(r_i, t) = 0. \quad (11)$$

This condition could be imposed by a hard wall inner circular boundary due to a central object. We discuss the inner boundary condition further in Section 5.7.

3 STANDARD MODEL

We start with a simple disc model that we define here. We later explore certain variations from this model. We adopt disc models in which $\gamma = 5/3$, $T \propto r^{-3/4}$, and $\Sigma \propto r^{-3/4}$. The density form corresponds to a steady state alpha disc with a constant value of alpha. In this model, the disc thickness-to-radius ratio is given by

$$H/r = h(r/r_{\text{res}})^{1/8}, \quad (12)$$

where $h = H/r$ evaluated at $r = r_{\text{res}}$. We do not consider any tapering of the disc density near the the outer edge. Some tapering is needed over a distance $\sim H$ to prevent pressure forces from causing the disc to become Rayleigh unstable, i.e., in order that the epicyclic frequency be real. We do not include tapering, in order to keep the standard model as simple as possible. In this paper, we consider discs with various h values, but take the r -dependence of T and Σ to be fixed.

We take the unit of length to be the binary separation d . We consider the effects the eccentricity instability at the 3:1 eccentric Lindblad resonance. For q small, the resonant radius is approximately given by

$$r_{\text{res}} = 3^{-2/3}(1 + q)^{-1/3}. \quad (13)$$

The 3:1 resonance strength χ in equation (9) is given by

$$\chi = 2.08 q^2 \Omega_b r_{\text{res}}, \quad (14)$$

where Ω_b is the binary orbital frequency (L91). This expression was independently confirmed by the particle model of Ogilvie (2007). The resonance width w_{res} depends on the disc sound speed and we take

$$w_{\text{res}} = h^{2/3} r_{\text{res}} \quad (15)$$

(see Meyer-Vernet & Sicardy 1987). We consider variations from this value of the width in Section 5.8.

We adopt a mass ratio $q = 0.1$ as a standard value. With this mass ratio, the disc outer radius determined by Paczynski's (1977) particle orbit intersection method is equal to 0.46. The disc radius given by the prescription suggested in Whitehurst & King (1991) evaluates to 0.53, which is 0.9 times the Roche lobe radius. We adopt a fiducial value of 0.5. The disc inner radius is chosen as 0.01 for numerical convenience to avoid the singularity at the disc center. Smaller inner disc radius values have little impact on the results presented here, as is discussed in Section 5.7.

In summary, we adopt a set of standard parameter values to model superhump binaries and later consider variations from some of these values. The standard model has $q = 0.1$, $h = 0.02$, $r_i = 0.01$, $r_o = 0.5$, $r_{\text{res}} = 0.466$, $\gamma = 5/3$, $T \propto r^{-3/4}$, and $\Sigma \propto r^{-3/4}$.

4 METHODS OF SOLUTION

Equation (1) and boundary conditions (10) and (11) are homogeneous and therefore permit the specification of the value of $E(r, 0)$ at some selected radius r . For the standard model we adopt a normalization

$$E(r_o, 0) = 1. \quad (16)$$

Of course, we are not suggesting that the actual eccentricity is unity. But, since the equations are linear, the solutions can be scaled linearly to any desired normalization.

Equation (1) can be solved by searching for eigenmodes in which

$$E(r, t) = E(r) \exp(i\omega t) \quad (17)$$

and complex frequency ω is the eigenvalue. The function $E(r)$ and eigenfrequency ω can be determined by shooting methods that satisfy the boundary and normalization conditions. Equation (1) is second order in space and can be integrated inward in radius starting at $r = r_o$ by using the two conditions, equations (10) and (16), and an assumed value for ω . Complex frequency ω is adjusted until the inner boundary condition, equation (11), is satisfied by using Newton's method. Another approach would be to discretise equation (1) in radius and solve the equations represented by a sparse matrix.

Such approaches have the drawback that there are many modes in the system and one must search for the physically relevant one that is the fastest growing. The shooting method is particularly prone to missing the fastest growing mode. The reason is that the guessed value for the eigenfrequency must be close to the value for the fastest growing mode. Otherwise, the method will typically converge on another eigenfrequency of the system.

We have instead opted to find the fastest growing mode by integrating equation (1) in space and time as a PDE. We apply the following initial condition

$$E(r, 0) = \cos \left[\frac{\pi}{2} \left(\frac{r_o - r}{r_o - r_i} \right) \right] \quad (18)$$

for $r_i \leq r \leq r_o$. This initial eccentricity satisfies boundary and normalization conditions (10), (11), and (16). Over time $E(r, t)/E(r_o, t)$ settles to an eigenfunction in which $\partial_t E/E$

is constant in space and is the complex eigenfrequency. This approach is computationally much slower than solving the eigenvalue problem with the shooting method, if one has a good initial guess for the eigenfrequency. We apply the eigenfrequency obtained from the time integration to the shooting method described above to verify its existence. We then smoothly vary other parameters such as q and h to rapidly obtain many other solutions by iteratively applying the eigenfrequency from the last obtained solution as the initial guess of the eigenfrequency for the next nearby set of parameters. In this way, we obtain a set of solutions, along a continuous branch that began with a fastest growing mode. There is no guarantee, however, that all solutions in this branch are the fastest growing for their set of parameters. Sufficiently nearby solutions are typically found to also be the fastest growing. However, as we will see, multiple branches occur that contain the fastest growing modes in different parameter regimes.

To integrate equation (1), we initially wrote a C program to implement the Crank-Nicholson method (e.g., Watanabe & Tsukada 2000). This method is unconditionally stable and fast, but produced some unwanted oscillations at high resolution, possibly as a consequence of Gudunov's Theorem (Wesseling 2001). Instead, we opted for the method of lines in Mathematica. With this method, the eccentricity is discretised in radius, producing a set of eccentricities $E_i(t)$, one at each radial grid point i . Equation (1) becomes to a set of coupled ODEs in time that are integrated by high order schemes. This method produced high resolution results.

Based on GO96, we express the growth rate for the standard model as

$$-Im(\omega) = \frac{\int r^{3/4} s(r) e^2(r) dr}{\int r^{3/4} e^2(r) dr} \simeq \frac{\chi}{\max(w_e, w_{\text{res}})} \left(\frac{e(r_{\text{res}})}{e_{\text{max}}} \right)^2, \quad (19)$$

where the integrals are taken over the disc from $r = r_i$ to $r = r_o$, e_{max} is the maximum eccentricity in the disc, and w_e is the radial width of the eccentricity distribution. This equation demonstrates the dependence of the growth rate on the properties of the eccentricity distribution.

5 RESULTS

5.1 Superhump Mode

The method of lines solution to equation (1) for the standard model, subject to initial condition (18) and boundary conditions (10) and (11), is plotted in Fig. 1. After a time of about 16 binary orbital periods, the eccentricity distribution settles into a mode. The values of the normalised eccentricity $e(r, t)/e(r_o, t)$ and the phase angle $\varpi(r, t)$ become nearly time-independent. The eccentricity growth rate $\partial_t e(r, t)/e(r, t)$ and precession rate $\partial_t \varpi(r, t)$ become independent of radius.

The eccentricity growth rate for the standard model is determined to be

$$\frac{\partial_t e(r, t)}{e(r, t)} = -Im(\omega) \simeq 0.10\Omega_b, \quad (20)$$

where $\omega = \partial_t E(r, t)/E(r, t)$.

This rapid growth rate is a consequence of the strong

overlap between the eccentricity distribution in the mode with the eccentricity driving by the resonance and the narrowness of the eccentricity distribution. From the figure, we estimate $w_e \simeq 0.1$ and $e(r_{\text{res}}) \simeq e_{\text{max}}$. Applying the parameters for the standard model ($q = 0.1$ and $r_{\text{res}} \simeq 0.466$), we obtain an estimated growth rate from equation (19) that is $-Im(\omega) \simeq 0.1\Omega_b$, in agreement with the rate obtained from the time-evolution solution, equation (20). Therefore, we find that the eccentricity is robustly excited in the outer parts of the disc. This calculation is telling us something that L91 did not, the effects of the eccentricity distribution on the growth rate. As we will see, the width of the eccentricity distribution w_e is a function of the system parameters and the growth rate itself.

The mode shown in the figure is termed the superhump mode. To understand its properties, we associate a timescale with each coefficient on the left-hand side of equation (1). The pressure, precession, and resonance instability timescales are estimated as $w_e^2 J/a$, J/b and r_o/χ , respectively. For the standard model, they crudely evaluate near the resonance to $10^3 w_e^2/(r_o^2 \Omega_b)$, $20/\Omega_b$, and $50/\Omega_b$, respectively. The effects of pressure act to spread the eccentricity distribution and balance against the effects of precession and resonance instability that will be shown to confine the eccentricity. The eccentricity distribution width w_e must be substantially smaller than r_o , so that the pressure timescale is comparable to the precession and instability timescales. Therefore, the eccentricity should be radially confined to a region smaller than the disc radius.

Notice that the phase of the mode decreases with radius, indicating that the mode is a trailing waveform. The radial wavelength is long, about equal to 0.3. Recall that the disc scale height is only about 2% of the disc radius or 0.01.

As outlined in Section 4, we apply the complex eigenfrequency obtained for the standard model to solve the mode equation by the shooting method. We then smoothly vary parameters to determine how the growth rate and modal structure varies as a function of various parameters, as will be described in the subsequent subsections.

5.2 Variations in q

We consider how the growth rate varies with binary mass ratio, q . As q varies, the radius of the 3:1 resonance varies slightly, according to equation (15). But since the resonance lies close to the disc outer edge, varying q alone would introduce an additional effect in changing the clearance between resonance and disc edge that we denote as

$$\Delta r_c = r_o - r_{\text{res}}. \quad (21)$$

We analyse the effects of changing the clearance Δr_c separately. Consequently, when varying q we also vary r_o so as to maintain a constant value $\Delta r_c = 0.5 - 0.466 = 0.034$. This means that r_o varies slightly with q .

We carried out a sequence of solutions to the modal equations using the shooting method for different binary mass ratios q . The results plotted in Fig. 2 show that the growth rate varies somewhat faster than q^2 . A quadratic dependence of the growth rate on q follows from the χ term (see equation (14)) in equation (19). The somewhat more rapid dependence is a consequence of additional mode confinement with increasing q (see Fig. 3). The confinement is

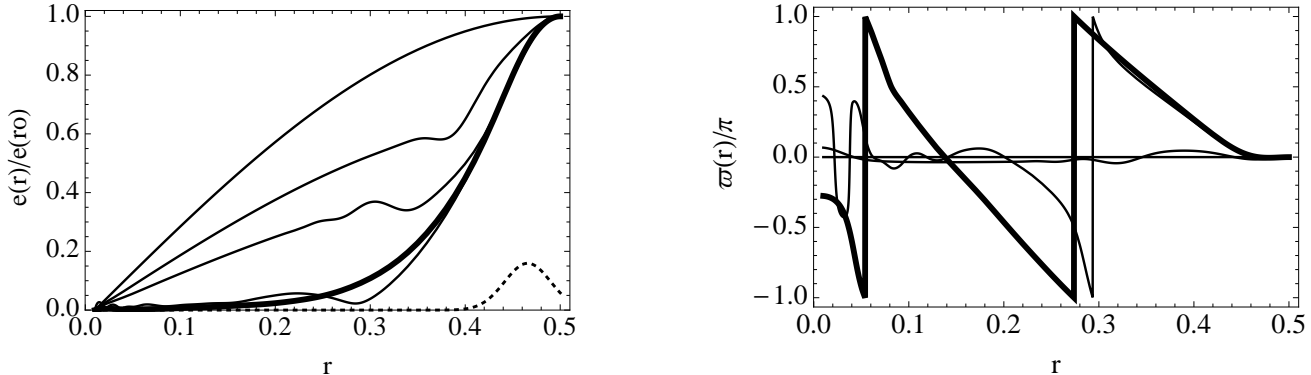


Figure 1. Evolution of eccentricity for the standard model ($q = 0.1, h = 0.02, r_o = 0.5$). The initial eccentricity distribution is of a cosine form, equation (18). Radius r is in units of the binary separation. *Left panel:* $e(r)$ at various times, normalised by its value at the disc outer edge. The curves monotonically drop in time at $r = 0.2$, corresponding to times of 0, 1, 2, 8 and 16 (thick line) binary orbits. The dotted curve is the 3:1 resonance instability factor $s(r)$ of equation (1) in units of Ω_b . *Right panel:* Phase angle (periapse angle) $\varpi(r)$ of the eccentricity in radians divided by π as a function of radius at various times. The curves monotonically increase in time at $r = 0.4$, corresponding to times of 0 (flat line of zero phase), 2, 8, and 16 (thick line) binary orbits.

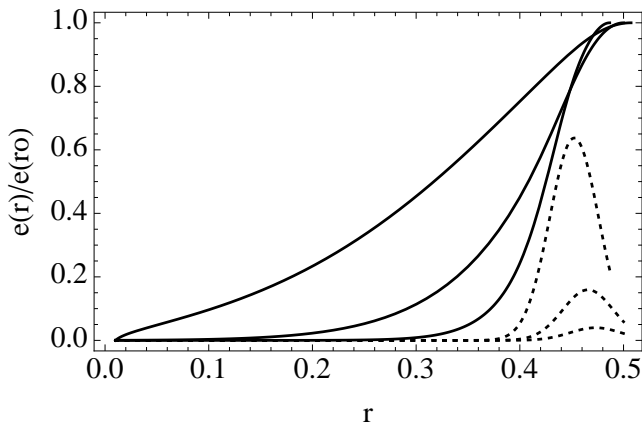


Figure 3. Eccentricity distributions for cases with standard parameters, but having different values of binary mass ratio q . The q values from the highest to lowest solid curves are 0.05, 0.1, and 0.2, respectively. The disc outer edge varies slightly with q from the standard value of 0.5, so that the distance from the resonance to the disc outer edge is maintained at a constant value. The dotted curves are the 3:1 resonance instability factors $s(r)$ of equation (1) in units of Ω_b for the same set of q values, where the peak values increase with increasing q . The eccentricity distributions narrow with increasing q , since the increasing growth rates cause the eccentricity to be more concentrated near the resonance.

a result of a competition between the pressure that spreads the distribution with the eccentricity growth that narrows the distribution to a region near the resonance.

5.3 Free eccentric mode

To determine the free eccentric mode corresponding to the superhump mode, we regarded q as fixed and constructed a sequence of models starting with the superhump mode and smoothly reduced the resonance strength χ (or $s(r)$) to zero. In that limit, we obtain a mode structure that is plotted in Fig. 4, along with the mode structure in the standard

model. Both modes are computed with the same disc outer radius equal to 0.5. The $\chi = 0$ mode corresponds to the fundamental (lowest order) free eccentric mode. Therefore, we see that the superhump mode results from the excitation of the free eccentric mode.

The additional mode confinement in the case of the growing mode can again be understood in terms of a competition between the radial pressure-induced propagation of eccentricity that acts to spread the mode and its growth that acts to localise the mode close to the 3:1 resonance that resides near the disc outer edge (the dotted curve in the figure). The confinement in the free mode case is shown below to be due to the effects of disc precession.

A previous estimate of eccentric disc free precession rate, based on the WKB theory of density waves, suggested

$$\omega = \dot{\omega}_g(r_o) - \frac{k^2 H^2}{2} \Omega(r_o), \quad (22)$$

where k is the radial wavenumber of the eccentric mode (Lubow 1992). This result demonstrates that pressure causes retrograde precession (by the second term on the right-hand side), opposite to the prograde precession due to the companion (the first term on the right-hand side). However, the magnitude of k was not determined.

We analyse the fundamental free precession mode for a cool disc by means of equation (1), together with equation (17) and the condition $s(r) = 0$. For a cool disc, we expect that the mode is confined to a small radial region near the disc outer edge and so $|dE/dr| \gg |E|/r$. In addition, we expect that $\omega \simeq \dot{\omega}_g(r_o)$. We apply these approximations to obtain

$$a(r_o) \frac{d^2 E}{dr^2} + J(r_o) (\dot{\omega}_g(r) - \omega) E(r) = 0. \quad (23)$$

We expand $\dot{\omega}_g(r)$ in a Taylor series to linear order about r_o and then have

$$r_o^2 \frac{d^2 E}{dr^2} + (c_0 + c_1 \Delta r) E(r) = 0, \quad (24)$$

where $\Delta r = r - r_o$,

$$c_0 = \frac{2}{\gamma} \left(\frac{r}{H} \right)^2 \frac{(\dot{\omega}_g(r_o) - \omega)}{\Omega}, \quad (25)$$

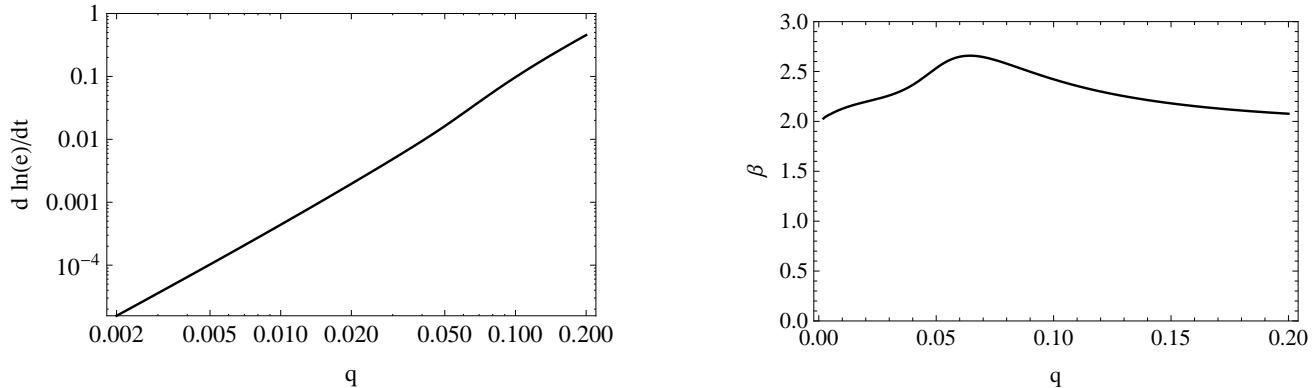


Figure 2. *Left panel:* Eccentricity growth rate in units of Ω_b , plotted against binary mass ratio q for the standard model. The disc outer edge varies slightly with q from the standard value of 0.5, so that the distance from the resonance to the disc outer edge is maintained at a constant value. *Right panel:* Plot of β , defined by $d \ln(e)/dt \propto q^\beta$ as a function of q based on the results of the left panel.

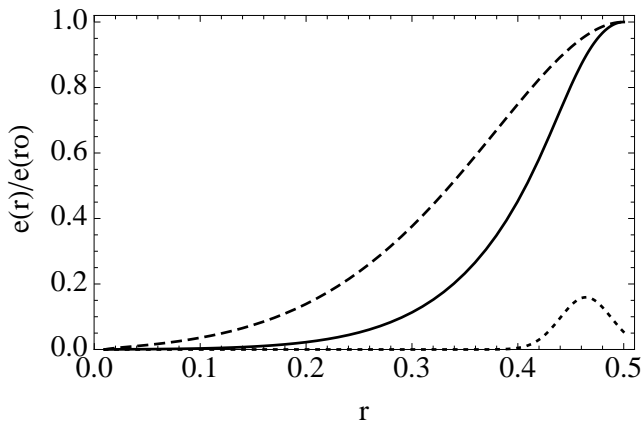


Figure 4. Eccentricity distribution for a system with standard parameters (solid line) and a system with zero resonance strength (dashed line), obtained through a sequence of models in which the resonance strength of the standard parameter case is smoothly lowered to zero. The dotted line is the 3:1 resonance instability factor $s(r)$ of equation (1) in units of Ω_b for the standard case (solid line). The 3:1 resonance in the outer parts of the disc acts to further confine the mode near the disc outer edge. The dashed curve is the fundamental free eccentric mode of the disc. It is that mode which is excited by the eccentricity instability to become the superhump mode.

and

$$c_1 = \frac{2}{\gamma} \left(\frac{r}{H} \right)^2 \frac{1}{\Omega} \frac{d\dot{\omega}_g}{dr}, \quad (26)$$

where c_1 and c_2 are evaluated at $r = r_o$. Applying equations (11) and (16), we obtain the solution to equation (24) as

$$E(r) = \frac{Ai(-c_2 - (r - r_o)/w_e)}{Ai(-c_2)}, \quad (27)$$

where Ai is the Airy function and

$$w_e^3 = \frac{\gamma}{2} \left(\frac{H}{r} \right)^2 \Omega \left(\frac{d\dot{\omega}_g}{dr} \right)^{-1} r_o^2. \quad (28)$$

Positive constant c_2 satisfies

$$Ai'(-c_2) = 0, \quad (29)$$

in order that the outer boundary condition (10) is satisfied. There are many (formally infinitely many) values of c_2 that satisfy equation (29), since Ai is oscillatory. Each such solution corresponds to a free eccentric mode. The number of nodes increases with increasing values of c_2 . The fundamental mode has the smallest value of c_2 and for this mode $c_2 \approx 1.019$.

The precession rate is given by

$$\omega = \dot{\omega}_g(r_o) - c_2 w_e \frac{d\dot{\omega}_g}{dr} \quad (30)$$

or

$$\omega \simeq \dot{\omega}_g(r_o - c_2 w_e). \quad (31)$$

Therefore, the precession rate for a cool disc with pressure is equal to the gravitational precession rate evaluated at a distance $c_2 w_e \simeq w_e$ inside the disc edge.

Equation (28) for width w_e demonstrates the competition between the sound speed or H that broadens the eccentricity distribution, and differential gravitational precession, $d\dot{\omega}_g/dr$, that acts to confine it. The analytic eccentricity distribution given by equation (27) roughly agrees with the numerically determined distribution for $H/r = 0.02$, but becomes fairly accurate for $H/r = 0.005$ (see Fig. 5). The precession rates given by equation (30) obtain similar levels of agreement with numerically determined values (see Fig. 6).

5.4 Variations in the disc outer radius

We analyse the eccentricity growth rate due to the 3:1 resonance as a function of the disc outer radius, or equivalently the clearance between the resonance and disc outer edge $\Delta r_c = r_o - r_{\text{res}}$, with all other parameters obtained from the standard model. For larger discs, other resonances can play a role, such as the 2:1 at $r = 0.61$ or $\Delta r_c = 0.15$, but we ignore such effects. The solid curve in Fig. 7 plots the eccentricity growth rate for the superhump mode as a function of Δr_c . If the disc resides sufficiently far inside the resonant radius, that is for $\Delta r_c < -w_{\text{res}} \sim -0.07$, then there is little overlap between the disc and the resonant region (i.e., where $s(r)$ is substantial; see equation (19)). The growth rates under such conditions are quite small. The growth rate rises rapidly for the disc edge close to, but inside the resonant radius (the

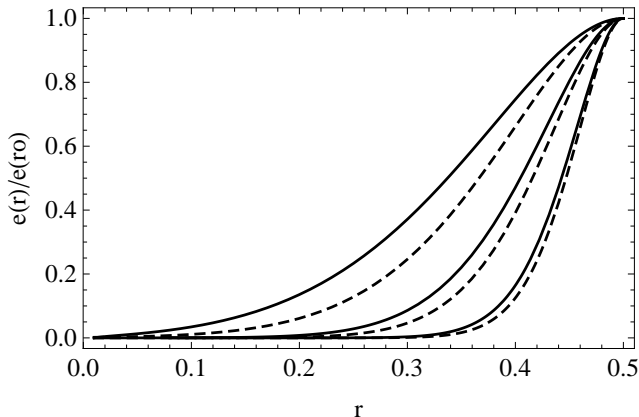


Figure 5. Eccentricity distributions for the fundamental free eccentric mode for systems with standard parameters, but different values of the dimensionless disc thickness H/r at the disc outer edge. The solid curves are determined by numerical solutions to equations (1) and (17), and the dashed curves are the analytic solutions for a cool disc given by equation (27). The lowest to highest dashed and solid curve pairs have values of $H/r = 0.005, 0.01$, and 0.02 , respectively.

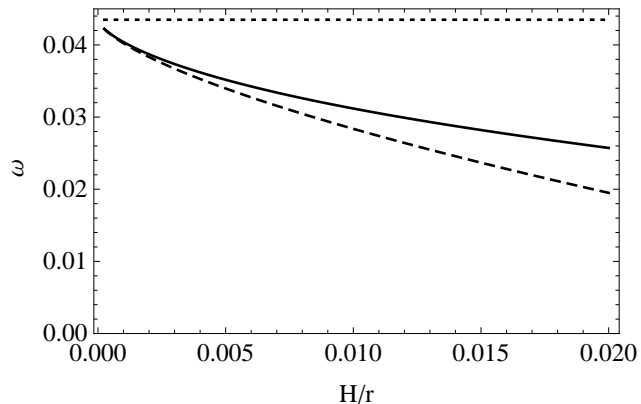


Figure 6. Eccentricity precession rate in units of Ω_b plotted against H/r , the disc thickness-to-radius ratio at the disc outer edge, for the standard model. The dashed line is given by the analytic formula, equation (30) for a cool disc, the solid line is determined by numerical solutions to equation (1), and the dotted line is the precession rate of a free particle at the disc edge, $\dot{\omega}_g(r_o)$.

peak of the dotted line), that is for $-0.05 < \Delta r_c < 0$. Consequently, the growth rate can be quite sensitive to the disc edge location.

We have idealised the gas distribution to be a smooth function of position that is sharply truncated at the disc edge. In a more realistic description, the disc density distribution tapers near the disc edge. The degree of overlap between the disc density distribution can be delicate in the case of superhump binaries. The reason is that the disc is truncated by tidal forces at a radius that is close to the 3:1 resonance. Furthermore, the extent of overlap with the resonant region will likely depend on the disc turbulent viscosity. We would qualitatively expect in the superhump binary case that the overlap, and consequently the eccentricity growth rate, would increase as the disc viscosity increases, since the

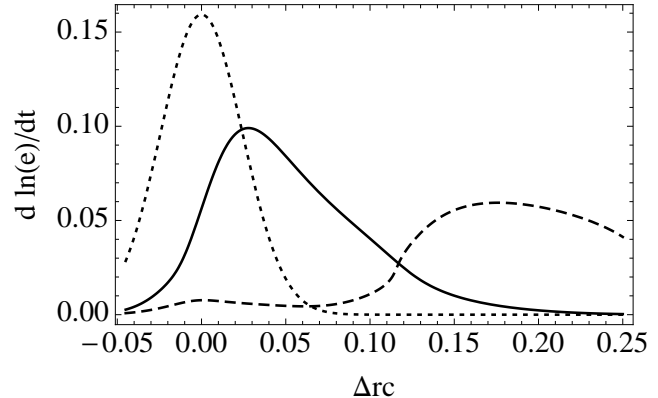


Figure 7. Eccentricity growth rate due to the 3:1 resonance in units of Ω_b plotted against Δr_c the difference between the disc outer radius and resonance radius. In the standard model $\Delta r_c \simeq 0.034$. The solid line is based on smooth continuation of the superhump mode. The dashed line is the growth rate for a higher order mode. The dotted curve is the 3:1 resonance instability factor $s(r_{\text{res}} + \Delta r_c)$ of equation (1) in units of Ω_b . Notice that for $\Delta r_c \gtrsim 0.12$ this alternative mode dominates, since it has a higher growth rate than the superhump mode.

disc tendency to spread outward is increased. Just that type of behavior was found in the simulations by Kley et al (2008).

For the standard model, $\Delta r_c \simeq 0.034$ and the growth rate is nearly optimal. For $\Delta r_c \gtrsim 0.05$ the growth rate drops because the peak amplitude of the mode occurs near the disc edge and is therefore further away from the resonant region (as seen in equation (19)). This can be seen in comparing for example the solid lines in Fig. 4 and Fig. 8 (that corresponds to $\Delta r_c \simeq 0.14$). The former has a stronger overlap with the resonance than the latter. So the growth rate in the standard disc case ($\Delta r_c \simeq 0.034$) is higher.

For $\Delta r_c \gtrsim 0.12$, the superhump mode is no longer the fastest growing. Such a large disc is unlikely to occur in typical superhump binaries, although it could occur in more extreme mass ratio systems. Under such a situation, the growth rates plotted by the dashed line in Fig. 7 dominate. The dashed line corresponds to a higher order eccentric mode. This mode (actually $e^2(r)$, see equation (19)) has a better overlap with $s(r)$, as seen in Fig. 8, and consequently grows faster than the superhump mode. In the absence of a companion, this higher order mode would decay faster in the presence of viscosity than the superhump mode would, due to its smaller scale spatial variations. Other modes could be expected to dominate under different conditions.

5.5 Variations in disc sound speed for $0.01 < h < 0.1$

We consider variations from the standard model in the disc gas sound speed or equivalently h , leaving all other parameters fixed. Fig. 9 shows that the eccentricity growth rate decreases with the dimensionless disc sound speed, as measured by dimensionless disc thickness h . Such behavior was found in simulations by Kley et al (2008). As seen in Fig. 10, this result can be understood in terms of the effects of the sound speed on mode confinement. As the disc sound speed increases, the mode spreads further until for $h \sim 0.05$ the

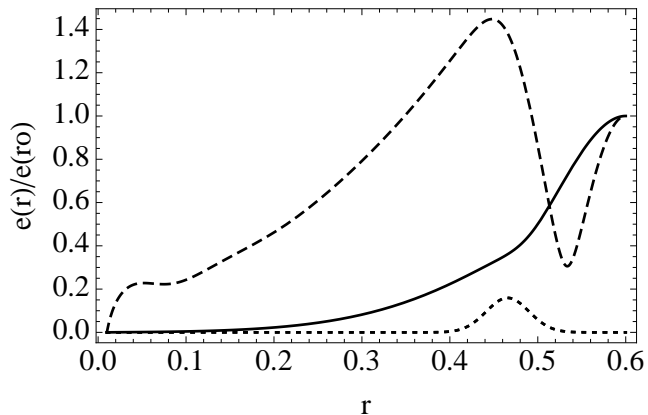


Figure 8. Eccentricity distributions for a system with standard parameters, but having disc outer radius $r_o = 0.6$ or $\Delta r_c \simeq 0.14$. The solid line plots the superhump mode, while the dashed line plots a higher order mode, corresponding to the rates plotted in solid and dashed curves respectively in Fig. 7. The dotted curve is the 3:1 resonance instability factor $s(r)$ of equation (1) in units of Ω_b . In this case, the higher order mode overlaps better with the instability factor $s(r)$ than the superhump mode and consequently has a faster growth rate, as seen in Fig. 7.

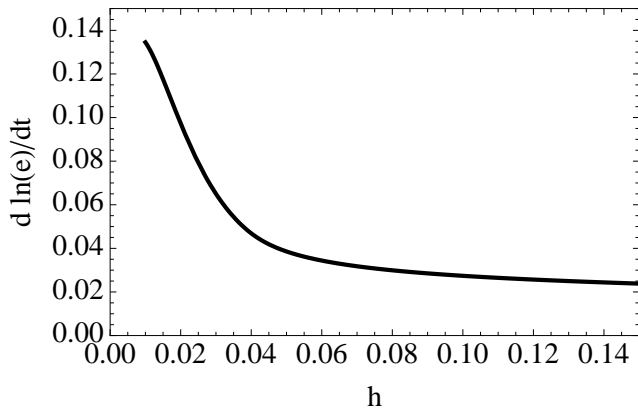


Figure 9. Eccentricity growth rate in units of Ω_b plotted against h , the disc thickness-to-radius ratio at the 3:1 resonance, for the standard model. The growth rate is higher at lower h because the eccentric mode becomes more confined near the resonance, as seen in Fig 10.

eccentricity is fairly uniform. The spreading is not simply a consequence of the broadening of the instability factor $s(r)$ with h (see equation (15)), since it does not spread as rapidly as the mode does with increasing h . Notice that for large h , the growth rate in Fig. 9 approaches a constant value. This behavior can be understood by the fact that in warmer discs the disc eccentricity becomes uniformly distributed in radius over the entire disc. We can then crudely take $w_e \sim r_{res}$ and $e_{res} \sim e_{max}$ in equation (19) and obtain a growth rate of $0.02\Omega_b$ that is in rough agreement with the figure for $h \sim 0.1$.

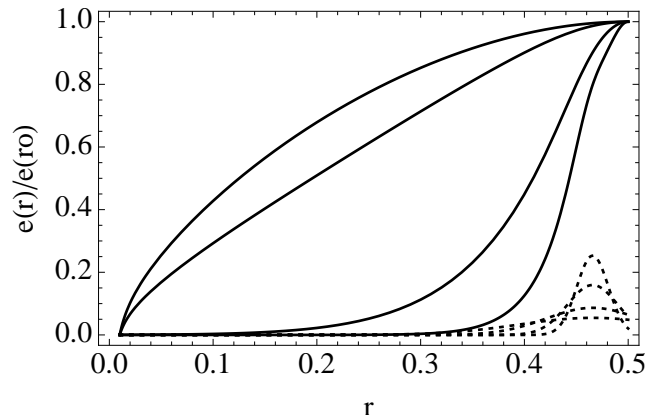


Figure 10. Eccentricity distributions for cases with standard parameters, but having different values of dimensionless disc sound speed h , the disc thickness-to-radius ratio at the 3:1 resonance. The values of h from the lowest to highest solid curves are 0.01, 0.02, 0.05, and 0.1, respectively. The dotted curves are the 3:1 resonance instability factors $s(r)$ of equation (1) in units of Ω_b for the same set of h values, where the peak values decrease with increasing h .

5.6 Variations in disc sound speed for $h < 0.01$

We analyse the behavior of the eccentricity growth rates and eccentricity distributions for cooler discs than were considered in Section 5.5. Fig. 11 shows that the growth rate rises abruptly with decreasing h , for $h \lesssim 0.007$. Fig. 12 shows that the nature of the eccentricity distributions change for sufficiently cool discs, since they detach from the disc outer edge. In the limit of a very cool disc, the resonance width $w_{res} = h^{2/3}r_{res}$ becomes smaller than Δr_c , the distance from the resonance to the disc edge. The distributions are then centered on the resonance. This description is valid provided that the resonance lies inside the disc, $r_{res} < r_o$. The rapid growth rates for cool discs are a consequence of the narrowing of the width of the eccentricity distribution (see equation (19)).

If $r_{res} > r_o$, the growth rate will drop to zero with decreasing sound speed, since there will be little overlap between the disc and the resonance. We assume in the remainder of this subsection that the resonance does lie within the disc, as follows from the parameters of the standard model.

We develop an analytic model in the very cool disc limit. In that limit, we have that $|dE/dr| \gg |E|/r$ and consequently equation (1) reduces in lowest order to

$$i\Omega(r_{res})\frac{d^2E}{dx^2} + s(x)E(x) = i\omega E(x), \quad (32)$$

where $x = \sqrt{2/\gamma}(r - r_{res})/H(r_{res})$. The boundary conditions for $E(x)$ are

$$E(-\infty) = E'(\infty) = 0 \quad (33)$$

and the normalization condition is chosen to be

$$E(0) = 1. \quad (34)$$

For a cool disc such that $H \ll w_{res}$, we approximate

the gaussian representation of $s(x)$ given by equation (9) as

$$s(x) \simeq \frac{\chi}{\sqrt{2\pi}w_{\text{res}}} \left(1 - \frac{\gamma}{2} \left(\frac{H}{w_{\text{res}}} \right)^2 x^2 \right). \quad (35)$$

The solution is given by

$$E(r) = \exp \left[-(1-i) \left(\frac{r-r_{\text{res}}}{w_e} \right)^2 \right] \quad (36)$$

and

$$\omega = -\frac{i\chi}{\sqrt{2\pi}w_{\text{res}}} \left(1 - \frac{(1+i)}{4} \left(\frac{w_e}{w_{\text{res}}} \right)^2 \right), \quad (37)$$

where

$$w_e = 2^{5/8} \gamma^{1/4} \pi^{1/8} \sqrt{H w_{\text{res}}} \left(\frac{\Omega w_{\text{res}}}{\chi} \right)^{1/4}. \quad (38)$$

The eccentricity $e(r) = |E(r)|$ is of gaussian form that is centered on the resonance and $\varpi(r) = (r-r_{\text{res}})^2/w_e^2$. The real radial velocity determined by equation (2) is $u'(r, \phi) = -r\Omega \exp(-(r-r_{\text{res}})^2/w_e^2) \sin((r-r_{\text{res}})^2/w_e^2 - \phi)$. For $r < r_{\text{res}}$, the phase term $(r-r_{\text{res}})^2/w_e^2 - \phi$ is constant for increasing r and decreasing ϕ . The waveform is then trailing for $r < r_{\text{res}}$ and leading for $r > r_{\text{res}}$. The width w_e involves a competition between the resonant growth factor χ and the gas sound speed, through its dependence on H and w_{res} . For w_{res} given by equation (15), it follows that w_e/w_{res} goes to zero in the limit that the gas sound speed (or H) goes to zero. That is, as the gas sound speed goes to zero, eccentricity distribution becomes concentrated into a region that is much smaller than the width of the resonance w_{res} . From equation (37), we see that eccentricity growth rate, $-Im(\omega)$, approaches $s(r_{\text{res}})$ for a cool enough disc that $w_e \ll w_{\text{res}}$. That is, the eccentricity growth rate approaches the growth rate of the instability at the resonance, as is consistent with equation (19).

Curiously, the detailed properties of the eccentricity distribution depend on the form taken for $s(x)$. If instead of a gaussian, we adopt a 'top-hat' form, then the results are somewhat different. Consider $s(x)$ defined by

$$s(x) = \frac{\chi}{2w_{\text{res}}} \quad (39)$$

for $\sqrt{\gamma/2}|x|H = |r-r_{\text{res}}| < w_{\text{res}}$ and zero otherwise. The solution to equation (32) is then given by

$$E(r) = \cos \left[\frac{\pi(r-r_{\text{res}})}{2w_{\text{res}}} \right] \quad (40)$$

for $|r-r_{\text{res}}| < w_{\text{res}}$ and zero otherwise, and

$$\omega = -\frac{i\chi}{2w_{\text{res}}} - \frac{\pi^2\gamma H^2\Omega}{8w_{\text{res}}^2}. \quad (41)$$

Unlike the gaussian case, the width of the eccentricity distribution does not get smaller than the width of the resonance in the very cool disc limit. In this case we have $\varpi(r) = 0$, unlike the gaussian case. While the gaussian case involved wrapped modes that were leading (trailing) for $r > r_{\text{res}}$ ($r < r_{\text{res}}$), the top-hat case contains equal amounts of leading and trailing waves at each radius. The growth rate is $-Im(\omega) = \chi/(2w_{\text{res}}) = s(r_{\text{res}})$. So again the eccentricity growth rate approaches the growth rate of the instability at the resonance.

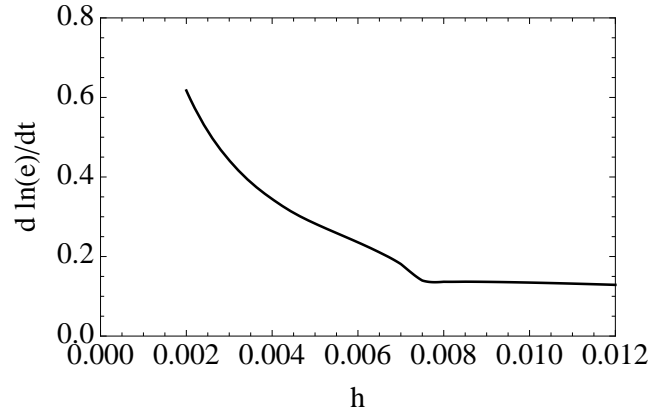


Figure 11. Eccentricity growth rate in units of Ω_b plotted against h , the disc thickness-to-radius ratio at the 3:1 resonance, for the standard model. This plot extends Fig. 9 to colder discs. For $h \lesssim 0.007$, the growth rate increases more rapidly with decreasing h , as the eccentric mode detaches from the disc outer edge and becomes centered on the resonance.

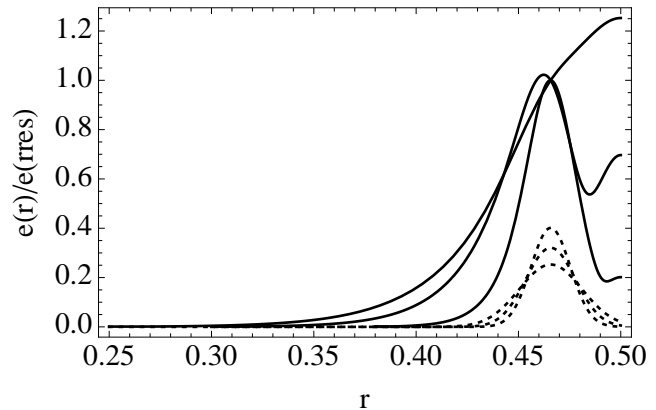


Figure 12. Eccentricity distributions, normalised by $e(r_{\text{res}})$, for cases with standard parameters, but having different values of dimensionless disc sound speed h , the disc thickness-to-radius ratio at the 3:1 resonance. The values of h from the lowest to highest solid curves at $r = 0.5$ are 0.005, 0.007, and 0.01, respectively. The dotted curves are the 3:1 resonance instability factors $s(r)$ of equation (1) in units of Ω_b for the same set of h values, where the peak values decrease with increasing h .

5.7 Variations of the inner boundary

We consider here the influence of both the location of the inner boundary and the form of the inner boundary condition on the eccentricity distribution and growth rate. For the cases described above with the standard model or colder discs, the inner boundary location typically has little influence. In such cases, the eccentricity distribution smoothly approaches zero with decreasing r far from the inner boundary. But for warmer discs, as may occur in the protostellar context, the eccentricity distribution is nonzero close to the inner boundary, as seen in Fig. 10. We consider then the case of a standard model disc having $h = 0.1$. The solid line plotted in Fig. 13 shows that the growth rate, even in this case, is insensitive to the inner boundary radius, provided that it is reasonably small, $r_i \lesssim 0.1$.

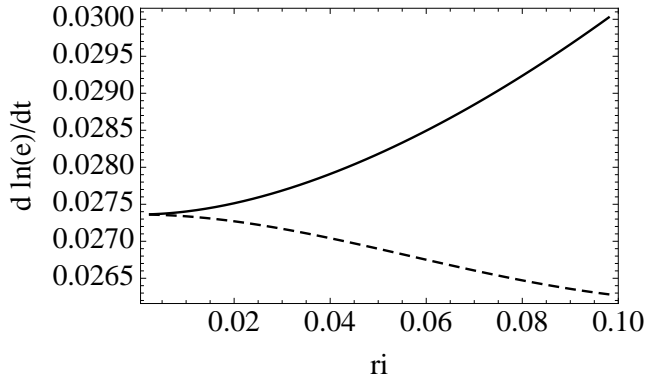


Figure 13. Eccentricity growth rate in units of Ω_b plotted against disc inner radius r_i for the standard model with $h = 0.1$. The solid (dashed) line is for the $E = 0$ ($\partial_r E = 0$) inner boundary condition. The growth rates converge as the disc inner radius goes to zero.

In the protostellar disc context, the disc may not extend to the central object, since there may be a hole near the disc center. It is then not obvious that the hard wall boundary condition (11) should apply. We consider then the effects of applying the inner boundary condition $\partial_r E = 0$, the same boundary condition we applied at the outer boundary. To explore these effects, we consider an expansion of equation (1) for small r with the standard model. We take r to be dimensionless, normalised by the binary separation. We apply equation (17) in the small r limit and obtain

$$r^2 E''(r) + 1.5rE'(r) - 0.9E(r) = 0. \quad (42)$$

The solution is written as

$$E(r) = c_1 (r^{s_1} + c_2 r^{-s_2}), \quad (43)$$

where $s_1 \approx 0.731$ and $s_2 \approx 1.23$. Constants c_1 and c_2 are determined by the inner boundary condition and the requirement that the solution join onto the solution outside of this region of small r . The hard wall ($E = 0$) boundary condition requires $c_2 = -r_1^{s_1+s_2}$. In the limit that r_1 goes to zero, we have that $E \propto r^{s_1}$.

The inner boundary condition $\partial_r E = 0$ requires that $c_2 = s_1 r_1^{s_1+s_2}/s_2$. We expect c_1 to be of order unity, since $|E| \sim 1$ where r of order unity. We then have that

$$E(r_i) = c_3 r_i^{s_1}, \quad (44)$$

for r_i small, where c_3 is a constant of order unity. Therefore, we have that the solution with the $\partial_r E = 0$ inner boundary condition approaches the solution with the hard wall $E = 0$ inner boundary condition in the limit that r_i goes to zero. That is, both cases have the same $E(r_i) = 0$ value in this limit. Consequently, the eccentricity distributions and growth rates are the same for both boundary conditions in the limit that the inner radius goes to zero. Fig. 13 shows that the growth rates are nearly the same for the two boundary conditions with small r_i and that they match as r_i goes to zero. Fig. 14 verifies that equation (44) holds well for numerical solutions of eccentric modes when r_i is small.

5.8 Variations of the resonance width

For the standard model, the resonance width given by equation (15) evaluates to $w_{\text{res}} \simeq 0.034$. Fig. 15 shows how the

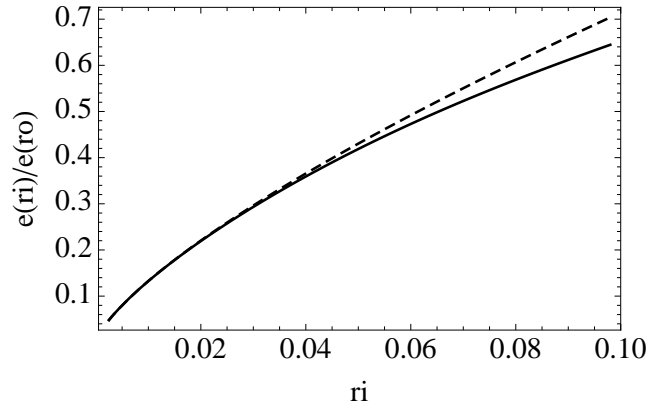


Figure 14. Eccentricity at the inner disc edge at a function of the inner disc radius r_i for the standard model with $h = 0.1$. The solid line is the result of numerical solutions for equations (1) and (17) with the condition $\partial_r E = 0$ applied at both the inner and outer boundaries. The dashed line is the prediction for $r_i \ll 1$ based on equation (44) with $c_3 = 3.82$.

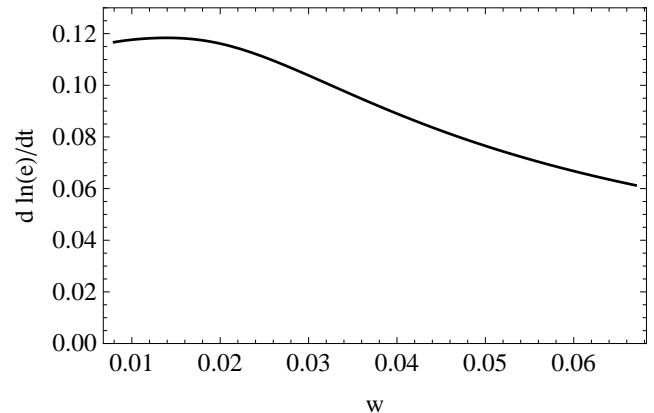


Figure 15. Eccentricity growth rate in units of Ω_b plotted against resonance width w with all other parameters given by the standard model. The growth rate declines somewhat for larger widths, as the resonance instability distribution $s(r)$ spreads beyond the disc outer edge.

eccentricity growth rate varies with w_{res} , where all other parameters are fixed at their standard values. For small w_{res} , the growth rate approaches a constant value as the resonance instability function $s(r)$ approaches the form of a Dirac delta function, as was used by GO06. The properties of the eccentricity distribution are insensitive to the resonance width. Recall that for the standard model, the resonance is located at distance $\Delta r_c \simeq 0.034 \simeq w_{\text{res}}$ from the disc outer edge. The portion of the resonance distribution $s(r)$ that lies outside the disc does not contribute to eccentricity growth. Consequently, the growth rate declines for $w_{\text{res}} \gtrsim \Delta r_c$.

6 SUMMARY AND DISCUSSION

We have investigated the evolution of discs subject to the eccentric instability caused by the 3:1 resonance. The 3:1 resonance is believed to be responsible for the eccentricity of discs in superhump binaries and the excitation mechanism

is understood in terms of a mode-coupling model (L91). The eccentricity growth rate is affected by the disc eccentricity distribution, principally by the radial width of the eccentric region and by the eccentricity at the resonance (see equation (19)). We explored the disc eccentricity distribution and its effect on the growth rate, as a function of system parameters using a linear equation developed by GO06, based on a two-dimensional disc model. The effects of turbulent viscosity on the eccentricity were ignored.

For typical superhump binary system parameters, the disc settles into a mode, the superhump mode, in which the eccentricity is concentrated in the outer parts of the disc (see Figs. 1 and 4). The mode results from the excitation of fundamental free eccentric mode. For the standard model defined in Section 3, the eccentricity growth rate is robust, since the mode overlaps well with the resonance and is concentrated near it. If the disc is somewhat smaller or larger than for the standard model, then the growth rate of the superhump mode is lower (Fig. 7). Similarly, if tidal forces lower the disc density in the region near the resonance, then we expect the growth rate to be reduced. In addition, the disc tapering needed to avoid Rayleigh instability at the outer edge could cause some density reduction in the resonant region and lower the growth rate.

The width of the eccentricity distribution is controlled by a competition between pressure forces that act to spread the mode and the eccentricity growth and differential precession that act to confine it (Figs. 3 and 10). The growth rate decreases with the increasing disc sound speed or disc thickness (see Fig. 9) and increases with binary mass ratio somewhat faster than quadratically (Fig. 2). Other eccentric modes can be excited under different conditions, such as larger or colder discs (Figs. 8 and 12).

Once the superhump feature is observed in binary systems, it is likely that the exponential growth phase, which occurs for small eccentricity, has ceased. In that case, the disc eccentricity may then be best described by the fundamental free eccentric mode, the free mode excited by the superhump instability. Equation (30) describes the free precession rate of a cool disc, subject to the approximations of this model.

Discs in young binary star systems of extreme mass ratio can similarly undergo eccentric instability. The eccentricity growth rates in units of the binary frequency are likely lower than in the superhump binary case, since protostellar discs are considerably warmer as measured by the dimensionless thickness h (see Fig. 9). Star-planet systems could similarly undergo such instability, although it likely involves the participation of other resonances that lie closer to the planet (Kley & Dirksen 2005, D'Angelo et al 2006). In that case also, we expect the eccentricity of the inner disc to be fairly broadly distributed because the mass ratio is much smaller and the disc thickness is larger than in the superhump binary case.

The effects of the disc vertical thickness, turbulent viscosity, and nonlinearity, omitted in this study, should be explored in the future (e.g., Ogilvie 2001).

7 ACKNOWLEDGMENTS

I have greatly benefitted from many discussions with Gordon Ogilvie and Jim Pringle on this topic. I am grateful for support from the IoA visitor program and NASA grant NNX07AI72G.

REFERENCES

- Borderies, N., Goldreich, P., & Tremaine, S. 1983, *AJ*, 88, 1560
D'Angelo, G., Lubow, S. H., & Bate, M. R. 2006, *ApJ*, 652, 1698
Goldreich, P., & Tremaine, S. 1979, *ApJ*, 233, 857
Goodchild, S., & Ogilvie, G. 2006, *MNRAS*, 381 (GO06)
Haswell, C. A., King, A. R., Murray, J. R., & Charles, P. A. 2001, *MNRAS*, 321, 475
Heemskerk M.H.M., 1994, *A&A*, 288, 807
Kley, W., & Dirksen, G. 2006, *A&A*, 447, 369
Kley, W., Papaloizou, J. C. B., & Ogilvie, G. I. 2008, *A&A*, 487, 671
Lubow, S. H. 1991a, *ApJ*, 381, 259 (L91)
Lubow, S. H. 1991b, *ApJ*, 381, 268
Lubow, S. H. 1992, *ApJ*, 398, 525
Murray, J. R. 2000, *MNRAS*, 314, L1
Neil, E. T., Bailyn, C. D., & Cobb, B. E. 2007, *ApJ*, 657, 409
Ogilvie, G. I. 2001, *MNRAS*, 325, 231
Ogilvie, G. I. 2007, *MNRAS*, 374, 131
Osaki, Y. 1985, *A&A*, 144, 369
Osaki, Y. 1996, *PASP*, 108, 39
Osaki, Y. 2003, *PASP*, 55, 841
Paczynski, B. 1977, *ApJ*, 216, 822
Papaloizou, J. C. B., Nelson, R. P., & Masset, F. 2001, *A&A*, 366, 263
Patterson J. et al., 2005, *PASP*, 117, 1204
Stehle, R. 1999, *MNRAS*, 304, 687
Vogt, N. 1982, *ApJ*, 252, 653
Watanabe, N., & Tsukada, M. 2000, *Phys. Rev. E*, 62, 2914
Warner, B. 1975, *MNRAS*, 170, 219
Wesseling, P. 2001, "Principles of Computational Fluid Dynamics," Springer-Verlag.
Whitehurst, R. 1988, *MNRAS*, 232, 35
Whitehurst R., & King A., 1991, *A&A*, 249, 25